

Short-range magnetic order in two-dimensional cobalt-ferrite nanoparticle assemblies

M. Georgescu,¹ J. L. Viota,² M. Klokkenburg,¹ B. H. Ern ,¹ D. Vanmaekelbergh,¹ and P. A. Zeijlmans van Emmichoven¹

¹*Faculty of Science, Utrecht University, P.O. Box 80000, 3508 TA Utrecht, The Netherlands*

²*Department of Applied Physics, School of Science, University of Granada, 18071 Granada, Spain*

(Received 4 October 2007; revised manuscript received 21 December 2007; published 23 January 2008)

Magnetic order in two-dimensional islands of spherical 21 nm cobalt-ferrite (CoFe₂O₄) nanoparticles is studied by magnetic force microscopy and spectroscopy. Images obtained at a temperature of 105 K clearly reveal the presence of repulsive and attractive areas on top of the islands. Monte Carlo simulations on hexagonal arrangements of nanoparticles have been carried out and are consistent with the experimental findings. The simulations show that the magnetization patterns are determined by a competition between interactions among the nanoparticle magnetic dipole moments and alignment of the individual moments along the easy axes of magnetization. At an elevated temperature of 500 K, it will be shown that dipole-dipole interactions lead to short-range ferromagnetic order, which fluctuates rapidly in time due to thermal excitations. Upon reduction of the temperature to 105 K, the dipole moments are forced toward the easy axes of magnetization, thereby increasing the amount of disorder.

DOI: [10.1103/PhysRevB.77.024423](https://doi.org/10.1103/PhysRevB.77.024423)

PACS number(s): 75.75.+a, 75.50.Tt, 75.60.Ch

I. INTRODUCTION

Magnetic nanoparticles have the potential to be utilized in several applications, with probably the best known being the use of thin films of magnetic nanoparticles in data storage devices.¹ Recently, it was demonstrated that magnetic nanoparticles may also be applied in magnetoelectronic devices.² Biomedicine is another example of an area of application of magnetic nanoparticles, for contrast agents in magnetic resonance imaging, for drug delivery, and for magnetic hyperthermia.^{3,4} The properties of the individual particles as well as their mutual interactions determine important features of the nanoparticle systems, such as storage capacity and switching field. Here, we demonstrate short-range magnetic order in a two-dimensional assembly of cobalt-ferrite nanoparticles.

Powerful chemical techniques have recently become available for the preparation of well-defined, magnetic nanoparticles with specific shape and size as well as with a high degree of crystallinity.^{5,6} Because of their nanoscale dimensions, it is energetically unfavorable for the particles to break up in more than one magnetic domain. The particles are, therefore, said to be single domain and they carry a large magnetic dipole moment. Three-dimensional systems, such as, e.g., dispersions of interacting magnetic nanoparticles, have been studied by a variety of experimental techniques^{7–12} and by simulations.^{13,14} In particular, their dynamics has been the subject of considerable interest: the interactions between the magnetic dipoles of the particles may lead to slow dynamics such as long relaxation times, aging, and memory effects.^{15–17} The results have been interpreted in terms of spin-glass-like behavior. Recently, such behavior was also observed in very dilute systems, where it was attributed to the energy barriers caused by the anisotropy of the individual particles.¹⁸

Dispersions with magnetic nanoparticles can be used to prepare dense, two-dimensional assemblies of particles.^{19,20} Since the particles contain a surfactant layer, they are generally separated by a few nanometers. This means that ex-

change interaction between nanoparticles, even in these dense assemblies, is negligible and their mutual interactions are, therefore, dominated by long-range dipole-dipole interactions. Spin-glass-like behavior has also been demonstrated for these two-dimensional systems of nanoparticles.^{21–23} It has, furthermore, been discussed that dipole-dipole interactions may lead to long-range order in the orientation of the dipoles.^{23,24} For two-dimensional systems of nanoparticles at vanishing temperature, calculations have shown that the structure of the assembly determines the type of order, with a hexagonal lattice resulting in ferromagnetic order and a square lattice in antiferromagnetic order.²⁵

The magnetocrystalline anisotropy energy of a magnetite nanoparticle, i.e., the energy originating in a misalignment of the magnetic dipole moment with respect to the easy axes of magnetization, is known to be low. This means that the magnetization pattern of an assembly of spherical magnetite nanoparticles is mainly determined by collective dipole-dipole interactions. We have recently shown that for two-dimensional islands of spherical 21 nm magnetite nanoparticles, the moments arrange themselves in flux-closure structures.²⁶ In the present study, results will be presented for two-dimensional islands of spherical 21 nm cobalt-ferrite nanoparticles. Unlike magnetite, the magnetocrystalline anisotropy energy of cobalt-ferrite is considerable and introduces energy barriers in the individual nanoparticles. The magnetization pattern, therefore, is determined by a competition between dipole-dipole interactions and alignment of the moments along the easy axes of magnetization. With the help of Monte Carlo simulations, the magnetization pattern of a hexagonal arrangement of nanoparticles has been studied. Significant differences have been observed for high and low temperatures, differences that are ascribed to the strong temperature dependence of the magnetocrystalline anisotropy energy of the particles.

II. EXPERIMENTAL METHODS

Spherical monodisperse cobalt-ferrite (CoFe₂O₄) nanoparticles were prepared according to a modified procedure

reported by Sun *et al.*,²⁷ by combining a high-temperature decomposition route with seed-mediated growth. Using this growth procedure, particles up to 25 nm could be prepared from small seed particles (5 nm). The particles were subsequently dispersed in cyclohexane in the presence of oleic acid and oleyl amine. The particles used in the present experiments had a diameter of 21.1 ± 2.7 nm as determined by transmission electron microscopy (TEM) using a Philips Tecnai 12 microscope at an accelerating voltage of 120 kV. The magnetic dipole moments of the particles were determined to be 1.1×10^{-18} A m². The moments were obtained from magnetization curves of a strongly diluted dispersion of the particles, and were measured at room temperature using an alternating gradient magnetometer [AGM; Micromag 2900 (Princeton Measurements Corporation)]. With the known value for the bulk magnetization of cobalt-ferrite of 4.25×10^5 A/m,²⁸ one finds that the moments correspond to a magnetic diameter of 17.0 nm. This reduced magnetic diameter is most likely caused by a weakly magnetic oxidic layer with a thickness of about 2 nm. The particles were deposited by placing a known volume of the nanocrystal dispersion on atomically flat highly oriented pyrolytic graphite (HOPG), followed by solvent evaporation (drop casting). Capillary forces active during the drying process led to the formation of two-dimensional, arbitrarily shaped, monolayer islands consisting of typically ten to several hundred nanoparticles. The samples were subsequently introduced into an ultrahigh vacuum chamber with a base pressure of better than 1×10^{-10} mbar and equipped with an OMICRON VT AFM/STM. The measurements have been carried out with commercially available conducting cantilevers, with Si tip of apex radius about 25 nm and covered with a magnetic 40-nm-thick CoCr film. The cantilevers have a resonance frequency of 70 kHz and a force constant of 2 N/m. Before the experiments were taken, the samples were annealed for about 2 h at a temperature of 500 K to prevent adherence of the tip to surfactant molecules at the nanoparticle surface. Without this procedure, tip crashes made scanning-probe experiments very difficult. We have no indications that this heating procedure led to sintering or growth of the nanoparticles.

The topography of the sample was studied with noncontact atomic force microscopy (nc-AFM) in frequency modulation mode. In this mode, the interaction between tip and sample induces a shift in resonance frequency of the oscillating cantilever. The amplitude of the cantilever was kept constant during the experiments and was estimated to be 10–20 nm. Since the amplitude is in the range of the characteristic length scale of the interaction forces, the measured frequency shift is directly proportional to the force exerted on the tip.²⁹ This implies that positive frequency shifts correspond to repulsion, negative frequency shifts to attraction. Contact-potential differences between tip and sample were corrected for by applying an appropriate potential to the tip. In addition to the nc-AFM experiments, magnetic force spectroscopy (MFS) and magnetic force microscopy (MFM) were carried out. In MFS, the frequency shift of the cantilever is measured as function of the tip-sample distance for specific lateral positions. In MFM, the frequency shift is measured while the sample is scanned at elevated height. In

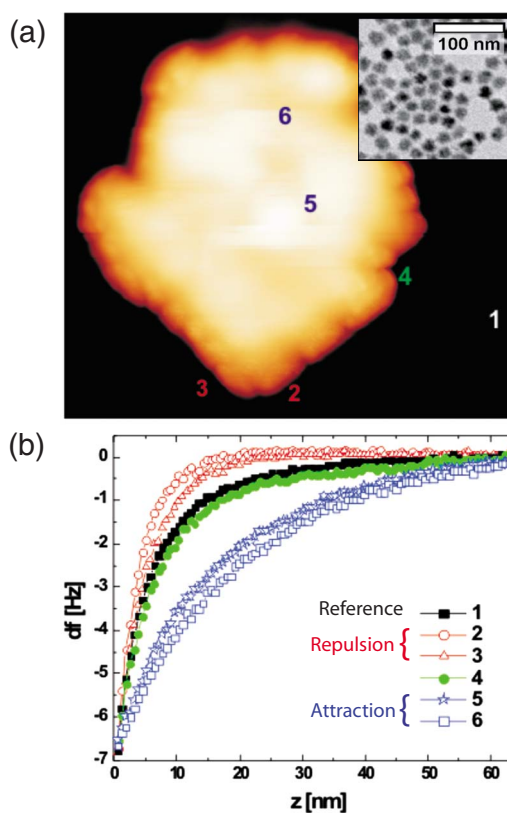


FIG. 1. (Color online) (a) AFM image taken at room temperature of a 380×310 nm² area of a HOPG surface with a monolayer island consisting of 70–90 21 nm spherical cobalt-ferrite nanoparticles (bright area). The image was taken at a frequency shift of -29 Hz. The vertical scale ranges from 0 nm (dark) to 26 nm (bright). The inset is a TEM image. (b) MFS curves measured at the positions indicated in (a).

this constant-height mode, the contribution from van der Waals interactions to the force is strongly reduced.

III. EXPERIMENTAL RESULTS

Experiments on monolayer islands of cobalt-ferrite nanoparticles were first carried out with the sample at room temperature. A typical result of a nc-AFM image is shown in Fig. 1(a). The size of the island indicates that it consists of approximately 70–90 nanoparticles. The TEM image (inset) illustrates the low polydispersity of the particles and their single-crystalline nature: the different contrast of the individual particles results from their crystalline orientations with respect to the electron beam. The MFM image is not shown, since on top of the island only strong attraction was observed with virtually no contrast variations. This indicates that with the magnetic tip directly above the island, its stray field significantly affects the magnetic moments of the nanoparticles. This behavior is confirmed by the force-spectroscopy curves shown in Fig. 1(b). Force curve 1 was measured above the HOPG substrate and shows attraction for all distances due to van der Waals forces. The attraction observed above the island of nanoparticles, on the other hand, is significantly stronger (curves 5 and 6). Weak repulsion

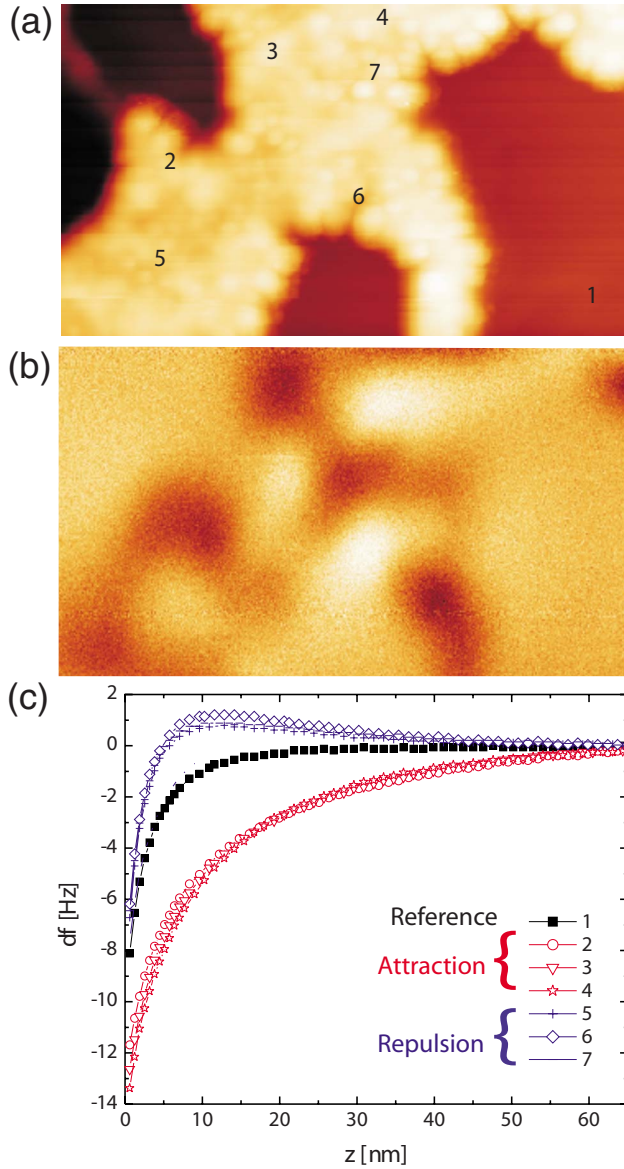


FIG. 2. (Color online) (a) AFM image taken at a temperature of 105 K of an area of $700 \times 385 \text{ nm}^2$ of a monolayer island of spherical 21 nm cobalt-ferrite nanoparticles (bright area) on top of a HOPG substrate. The image was taken at a frequency shift of -10 Hz . The vertical scale ranges from 0 nm (dark) to 35 nm (bright). (b) MFM image of the same area taken in constant-height mode at a distance of 40 nm above the HOPG substrate. The vertical scale ranges from -4 Hz (dark) to 2 Hz (bright). (c) Force curves measured at the positions indicated in (a).

was observed only at the edge of the island as illustrated by curves 2 and 3. The magnetic interaction for these curves, which is obtained when the van der Waals interaction is subtracted, seems to be repulsive for virtually all distances. It should be noted that, as illustrated by curve 4, at the edge the measured interaction between tip and nanoparticles is not always repulsive. The results shown in Fig. 1 are reminiscent of what we observed at two-dimensional islands of magnetite nanoparticles.²⁶ The interpretation, therefore, can be along the same lines: the dipole moments of the individual particles are blocked due to dipole-dipole interactions and, for cobalt-

ferrite, also due to anisotropy. This may lead to repulsion of the magnetic moment of the tip at the edge of the island. Directly above the island, however, the stray field of the tip is sufficiently strong to reorient the dipole moments of the nanoparticles leading to long-range attraction. Comparison with our previous magnetite results (Fig. 3 in Ref. 26) shows both repulsion and attraction measured at cobalt-ferrite islands are significantly weaker. This is consistent with the measured value for the magnetic moment of the cobalt-ferrite nanoparticles that is a factor of 2 smaller.

For cobalt-ferrite, it is well known that the anisotropy energy strongly increases with decreasing temperature.³⁰ Several experiments were carried out at temperatures significantly below room temperature. A typical result obtained at an island of 150–200 cobalt-ferrite nanoparticles at a temperature of 105 K is shown in Fig. 2. MFM experiments were carried out in constant-height mode at a distance of 40 nm above the HOPG substrate. The MFM image shown in Fig. 2(b) clearly shows that above the island, not only attractive (dark) but also repulsive (bright) areas are present. This result is markedly different from the results obtained at room temperature, and is supported by force-spectroscopy experiments taken in the attractive as well as in the repulsive areas [Fig. 2(c)]. Obviously, at this reduced temperature, the anisotropy energy barriers in the particles are sufficiently high to prevent reorientation of the dipole moments by the stray field of the tip. The repulsive and attractive areas are of rather arbitrary shape and typically contain of the order of 10–20 nanoparticles. With the finite size of the tip limiting the lateral resolution to approximately 40 nm, the actual size of the areas may be somewhat smaller. Similar results were obtained for islands of different size and at other temperatures (70–135 K).

IV. NUMERICAL METHODS

To study the origin of the repulsive and attractive areas in the measured MFM images, Monte Carlo simulations have been carried out on a hexagonal arrangement of 60 nanoparticles. This area is of similar dimensions as, e.g., the region in the lower left corner of the experimental image shown in Fig. 2(a). The most important energies that determine the magnetic structure of the sample are the dipole-dipole energy of all pairs of particles and the anisotropy energy of all particles. The dipole-dipole energy E_{dd} is given by

$$E_{dd} = -\frac{\mu_0}{4\pi} \sum_{i < j} \left(\frac{3(\vec{m}_i \cdot \hat{r}_{ij})(\vec{m}_j \cdot \hat{r}_{ij}) - (\vec{m}_i \cdot \vec{m}_j)}{r_{ij}^3} \right), \quad (1)$$

with \vec{m}_i and \vec{m}_j the magnetic dipole moments of the particles i and j , r_{ij} the distance between particles i and j , and \hat{r}_{ij} the unit vector pointing from particle i to particle j . Concerning anisotropy, we assume that magnetocrystalline anisotropy dominates and that the cobalt-ferrite nanoparticles have cubic anisotropy, with the first anisotropy constant $K_1(T)$ being temperature dependent.³⁰ Higher-order anisotropy terms were not taken into account in the simulations. This yields the anisotropy energy³¹ E_{an}

$$E_{an} = K_1(T)V \sum_i \left(\frac{m_{i1}^2 m_{i2}^2 + m_{i1}^2 m_{i3}^2 + m_{i2}^2 m_{i3}^2}{m_i^4} \right), \quad (2)$$

with m_{ij} , for $j=1,2,3$, the components of the magnetic moments along the cubic axes and V the volume of the particles. For the temperature dependence of $K_1(T)$, we used the empirical Brückhatov-Kirenski relation for bulk cobalt-ferrite³²⁻³⁴

$$K_1(T) = K_1(0)\exp(-\alpha T^2), \quad (3)$$

with the temperature T in K, $K_1(0) = 19.6 \times 10^5 \text{ J/m}^3$, and $\alpha = 1.9 \times 10^{-5}$.³⁰ The anisotropy constant being positive implies that the easy axes of magnetization of a nanoparticle coincide with its three cubic crystal axes. E_{an} becomes 0 for a magnetic moment aligned with one of the easy axes, and positive for all other directions.

The orientation of the crystal axes of each particle was taken to be random with respect to the orientation of the axes of all other particles. During the simulations, the particles were not allowed to move: only the moments rotate inside the particles (Néel rotation). Assuming either a random configuration of initial dipole moments or a configuration calculated in a previous run, the direction of all moments was varied in a random way. If, upon variation of an individual moment, the energy of the system was lower, the step was accepted; if the energy was higher, the step was only accepted with probability equal to the Boltzmann factor [$\exp(-\Delta E/k_B T)$, with ΔE the change in energy of the system]. In each run, all moments were varied 10^4 times. With a typical attempt frequency for variation of the moments of $10^9 - 10^{10} \text{ s}^{-1}$,²³ this means that the simulation takes place on a time scale of the order of $1 - 10 \mu\text{s}$. Assuming the magnetic moment of the tip to be perpendicular to and pointing toward the sample, the force exerted on the tip can directly be calculated from the configuration of moments of the nanoparticles. To be able to compare to experimental MFM images, the force was calculated on a two-dimensional grid in a plane parallel to the island of nanoparticles and subsequently transformed to frequency shift.²⁹ For the absolute value of the moment of the tip, we used $2.5 \times 10^{-17} \text{ A m}^2$. This value gives frequency shifts of a few hertz as observed in the experiments, and is close to values reported in the literature for similar tips.³⁵

V. NUMERICAL RESULTS AND DISCUSSION

As discussed in Sec. II, before carrying out the experiments, the samples were annealed at 500 K. We first present results for simulations at this elevated temperature. A typical result is shown in Fig. 3(a), for which a random configuration of initial dipole moments was used. The arrows in the figure correspond to the in-plane components of the moments. Calculated dipole-dipole energies and anisotropy energies are tabulated in Table I. The image reveals that, although some of the moments have significant components out of plane, most of them arrange themselves in plane. The gray areas, where the moments point in (close to) the same direction, illustrate a few of the areas where short-range fer-

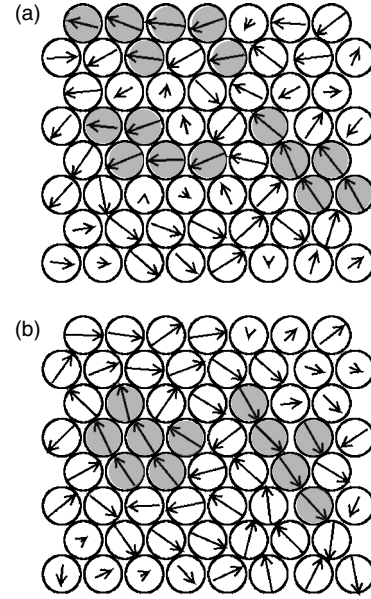


FIG. 3. (a) Calculated configuration of magnetic moments for a hexagonal arrangement of 60 spherical 21 nm cobalt-ferrite nanoparticles at a temperature of 500 K. The arrows indicate the direction of the magnetic moments with their length representing the in-plane components (when an arrow is as large as a nanoparticle, this means that its moment is fully in plane). The gray areas indicate a few of the areas where short-range order is present. (b) Simulated results after another 10^4 steps using the same easy axes for magnetization for all particles and the final moments as shown in Fig. 3(a) as input.

romagnetic order is present. The order originates in dipole-dipole interactions, which tend to bring the system in a flux-closure-type arrangement.²⁶ Magnetocrystalline anisotropy at this elevated temperature also plays a role (see Table I), although its energy barriers obviously do not prevent short-range order to be formed. This, in fact, is not surprising when thermal energy at this temperature, $k_B T \approx 43 \text{ meV}$, is compared to one of the energy barriers in the particles: for rotation of the dipole moment in a plane containing two of the three easy axes of magnetization, the barrier^{36,37} becomes $K_1(T)V/4 \approx 128 \text{ meV}$. For the calculated magnetization pat-

TABLE I. Calculated average dipole-dipole energies and magnetocrystalline anisotropy energies per particle ($E_{dd}^p = E_{dd}/60$ and $E_{an}^p = E_{an}/60$, respectively). The second column gives the initial configuration of moments used (either random or from a previous run). Also given is the anisotropy constant multiplied by the volume of a particle. The energies in the last three columns are given in meV.

	Initial moment	T (K)	$K_1(T)V$	E_{dd}^p	E_{an}^p
Fig. 3(a)	Random	500	513	-90	+37
Fig. 3(b)	Previous	500	513	-93	+35
Fig. 4(a)	Random	500	513	-95	+35
Fig. 4(b)	Previous	105	4.9×10^4	-75	+9.2
Not shown	Random	105	4.9×10^4	-2.2	+8.5

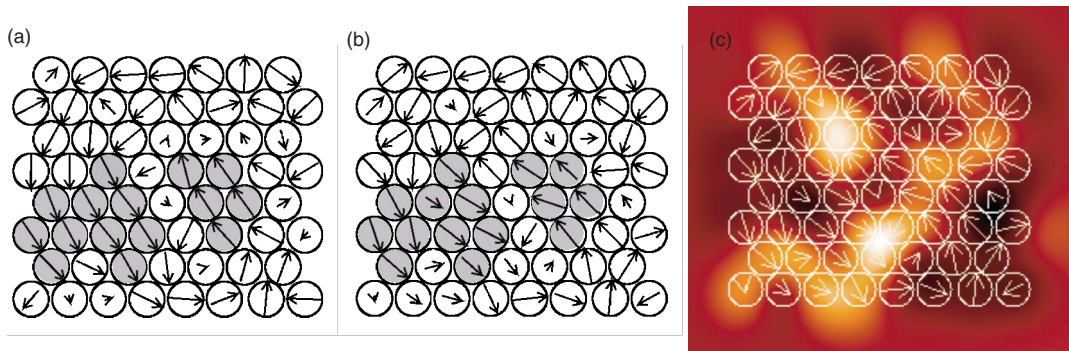


FIG. 4. (Color online) (a) Calculated configuration of magnetic moments for an arrangement of 60 spherical 21 nm cobalt-ferrite nanoparticles at a temperature of 500 K. An arbitrary configuration of initial moments was used at the start of the simulations. The arrows indicate the direction of the magnetic moments, with their lengths representing the in-plane components (when an arrow is drawn as large as a nanoparticle, this means that its moment is fully in plane). The gray areas indicate a few of the areas where local order is present. (b) Calculated configuration of magnetic moments at a temperature of 105 K. The final moments as shown in (a) were used as input and, in addition, the easy axes of magnetization were kept the same. (c) Same results as shown in (b) with, in addition, the MFM signal calculated for a tip moving at a distance of 40 nm above the substrate (area $235 \times 210 \text{ nm}^2$). Colors range from dark (-2.1 Hz) to bright ($+2.3 \text{ Hz}$).

tern, the average dipole-dipole energy per particle amounts to a value only slightly larger than $2k_B T$. This means that even in areas where short-range order is present and where the dipole-dipole energy per particle may be somewhat larger, the individual moments will rapidly fluctuate by thermal excitations. This is illustrated by Fig. 3(b), which is the result of the simulation shown in Fig. 3(a) after another 10^4 steps. Clearly, the magnetization pattern has completely changed. These rapid thermal fluctuations are also the cause that flux closure for the whole system of nanoparticles is not reached.

We next discuss the behavior of the dipole moments when the particles are cooled to a temperature of 105 K. The role played by magnetocrystalline anisotropy is expected to significantly increase because of its exponential dependence on temperature [see Eq. (3)]. To mimic the experimental procedure as good as possible, first, a simulation was carried out at 500 K; the final moments were subsequently used as input for the simulation at 105 K. The positions of the particles as well as their easy axes of magnetization were the same in both simulations, thereby assuming that the particles did not move during the cooling process. Typical results are shown in Figs. 4(a) and 4(b), respectively, for 500 and 105 K. In the simulation at 500 K, several areas with short-range ferromagnetic order can be identified. Upon cooling, these areas seem to preserve their short-range order, but the moments become more disordered and the average dipole-dipole energy per particle slightly decreases (see Table I). Since, at this reduced temperature, the anisotropy constant has increased by almost 2 orders of magnitude, this behavior can easily be understood in terms of a reorientation of the dipole moments in the direction of one of their easy axes of magnetization. In this way, the average anisotropy energy per particle remains low (even lower than the value at 500 K, see Table I). Since the energy barriers are very high compared to $k_B T$, they are virtually impossible to cross by thermal excitations and the magnetization pattern, therefore, will be thermally stable. Important to note is that the presence of short-range order at this reduced temperature is a consequence of

the order already present at 500 K, with the dipole moments of the nanoparticles remaining at an “energetically favorable side” of the energy barriers during the cooling process. To confirm this picture, we carried out simulations at 105 K that were started with an arbitrary set of initial moments. The dipole moments, indeed, were not able to cross the energy barriers, resulting in the absence of short-range order and in an average dipole-dipole energy per particle very close to 0 (see Table I).

The results of the simulation at 105 K are shown again in Fig. 4(c), together with, in the background, the calculated MFM signal. Bright areas in the image indicate repulsion; dark areas attraction. An important observation is that bright and dark areas in the MFM image cannot be related, one to one, to areas of short-range order or to transitions between such areas [compare, e.g., the location of the gray areas in Fig. 4(b) to the MFM spots in Fig. 4(c)]. This shows that an interpretation of a MFM image of a system of interacting dipoles is less straightforward than the interpretation of an image of magnetic domains in ferromagnetic materials.³⁸ The size of repulsive and attractive areas in Fig. 4(c) is in the order of 5–10 nanoparticles. This size, as well as the rather arbitrary shape of the areas, is consistent with the experimental results shown in Fig. 2(b). We conclude that the contrast in the experimental MFM image originates in configurations of magnetic dipoles similar to the ones in the simulations.

We finally discuss some important implications of the present work. Zero-field-cooled experiments on assemblies of nanoparticles have frequently been used to determine values for nanoparticle magnetic moments.²³ Moments considerably larger than any possible moment of the individual particles were recently reported.^{39,40} The results were interpreted in terms of strongly interacting dipoles that increase the observed “effective” moment. The areas of short-range order in this work correspond to the “correlated clusters” as discussed in Ref. 40. We have, furthermore, shown that repulsive and attractive areas in MFM images of interacting dipoles cannot directly be related to ordered areas. This should be taken into account in the interpretation of MFM

images of one- and two-dimensional assemblies of interacting nanoparticles as discussed elsewhere.^{41,42} We finally propose that the occurrence of areas of short-range order in two-dimensional assemblies of nanoparticles may be of use for magnetic data storage purposes. It has been discussed elsewhere¹ that for the use of two-dimensional assemblies of magnetic nanoparticles, it would be “highly desirable that the ordered particles have a common magnetic easy axis.” The present results illustrate that in assemblies of nanoparticles with cubic anisotropy, a relatively high degree of short-range order can be achieved without their easy axes being aligned. This may open interesting possibilities for future application of such particles.

VI. CONCLUSIONS

We have shown that the magnetization pattern of an assembly of cobalt-ferrite nanoparticles is determined by the competition between collective dipole-dipole interactions

and alignment of the dipole moments along the easy axes of magnetization. The role of thermal fluctuations on the magnetization pattern was discussed. The observed, rapidly fluctuating, short-range ferromagnetic order at elevated temperature originates in an average dipole-dipole interaction strength, which is only a factor of 2 larger than thermal energy. Upon cooling the assembly of nanoparticles, short-range order is preserved, but with a significant increase in the amount of disorder. It was finally shown that, for interacting dipoles, it is not allowed to make a one-to-one correspondence between contrast in a measured MFM image and ordered areas.

ACKNOWLEDGMENTS

This work is supported by the “Stichting voor Fundamenteel Onderzoek der Materie (FOM),” which is financially supported by the “Nederlandse Organisatie voor Wetenschappelijk Onderzoek (NWO).”

-
- ¹B. D. Terris and T. Thomson, *J. Phys. D* **38**, R199 (2005).
²H. Zeng, C. T. Black, R. L. Sandstrom, P. M. Rice, C. B. Murray, and S. Sun, *Phys. Rev. B* **73**, 020402(R) (2006).
³Q. A. Pankhurst, J. Connolly, S. K. Jones, and J. Dobson, *J. Phys. D* **36**, R167 (2003).
⁴P. Tartaj, *Curr. Nanosci.* **2**, 43 (2006).
⁵S. Sun, C. B. Murray, D. Weller, L. Folks, and A. Moser, *Science* **287**, 1989 (2000).
⁶V. F. Puentes, K. M. Krishnan, and A. P. Alivisatos, *Science* **291**, 2115 (2001).
⁷W. Luo, S. R. Nagel, T. F. Rosenbaum, and R. E. Rosensweig, *Phys. Rev. Lett.* **67**, 2721 (1991).
⁸J. García-Otero, M. Porto, J. Rivas, and A. Bunde, *Phys. Rev. Lett.* **84**, 167 (2000).
⁹J. B. Kortright, O. Hellwig, K. Chesnel, S. Sun, and E. E. Fullerton, *Phys. Rev. B* **71**, 012402 (2005).
¹⁰S. Mørup and E. Tronc, *Phys. Rev. Lett.* **72**, 3278 (1994).
¹¹C. Cannas, A. Musinu, G. Piccaluga, D. Fiorani, D. Peddis, H. K. Rasmussen, and S. Mørup, *J. Chem. Phys.* **125**, 164714 (2006).
¹²F. Brem, L. Tiefenauer, A. Fink, J. Dobson, and A. M. Hirt, *Phys. Rev. B* **73**, 224427 (2006).
¹³D. Kechrakos and K. N. Trohidou, *Phys. Rev. B* **58**, 12169 (1998).
¹⁴R. W. Chantrell, N. Walmsley, J. Gore, and M. Maylin, *Phys. Rev. B* **63**, 024410 (2000).
¹⁵C. Djurberg, P. Svedlindh, P. Nordblad, M. F. Hansen, F. Bødker, and S. Mørup, *Phys. Rev. Lett.* **79**, 5154 (1997).
¹⁶J. O. Andersson, C. Djurberg, T. Jonsson, P. Svedlindh, and P. Nordblad, *Phys. Rev. B* **56**, 13983 (1997).
¹⁷Y. Sun, M. B. Salamon, K. Garnier, and R. S. Averback, *Phys. Rev. Lett.* **91**, 167206 (2003).
¹⁸M. Sasaki, P. E. Jönsson, H. Takayama, and H. Mamiya, *Phys. Rev. B* **71**, 104405 (2005).
¹⁹V. F. Puentes, K. M. Krishnan, and A. P. Alivisatos, *Appl. Phys. Lett.* **78**, 2187 (2001).
²⁰T. Fried, G. Shemer, and G. Markovich, *Adv. Mater. (Weinheim, Ger.)* **13**, 1158 (2001).
²¹P. Poddar, T. Telem-Shafir, T. Fried, and G. Markovich, *Phys. Rev. B* **66**, 060403(R) (2002).
²²D. Farrell, Y. Cheng, R. W. McCallum, M. Sachan, and S. A. Majetich, *J. Phys. Chem. B* **109**, 13409 (2005).
²³S. A. Majetich and M. Sachan, *J. Phys. D* **39**, R407 (2006).
²⁴S. Mørup and G. Christiansen, *J. Appl. Phys.* **73**, 6955 (1993).
²⁵V. Russier, *J. Appl. Phys.* **89**, 1287 (2001).
²⁶M. Georgescu, M. Klokkenburg, B. H. Erné, P. Liljeroth, D. Vanmaekelbergh, and P. A. Zeijlmans van Emmichoven, *Phys. Rev. B* **73**, 184415 (2006).
²⁷S. Sun, H. Zeng, D. B. Robinson, S. Raoux, P. M. Rice, S. X. Wang, and G. Li, *J. Am. Chem. Soc.* **126**, 273 (2004).
²⁸R. E. Rosensweig, *Ferrohydrodynamics* (Cambridge University Press, Cambridge, England, 1985).
²⁹J. E. Sader and S. P. Jarvis, *Phys. Rev. B* **70**, 012303 (2004).
³⁰V. Blaskov, V. Petkov, V. Rusanov, L. M. Martinez, J. S. Muñoz, and M. Mikhov, *J. Magn. Magn. Mater.* **162**, 331 (1996).
³¹A. Hubert and R. Schäfer, *Magnetic Domains* (Springer-Verlag, Berlin, 1998).
³²N. L. Brückhatov and L. V. Kirensky, *Phys. Z. Sowjetunion* **12**, 602 (1937).
³³N. L. Brückhatov and L. V. Kirensky, *Tech. Phys. (U.S.S.R.)* **5**, 171 (1938).
³⁴H. Shenker, *Phys. Rev.* **107**, 1246 (1957).
³⁵M. Raşa, B. W. M. Kuipers, and A. P. Philipse, *J. Colloid Interface Sci.* **250**, 303 (2002).
³⁶N. Moumen, P. Bonville, and M. P. Pileni, *J. Phys. Chem.* **100**, 14410 (1996).
³⁷M. P. Pileni, *Adv. Funct. Mater.* **11**, 323 (2001).
³⁸U. Hartmann, *Annu. Rev. Mater. Sci.* **29**, 53 (1999).
³⁹S. Trudel and R. H. Hill, *Polyhedron* **26**, 1863 (2007).
⁴⁰S. Trudel, C. H. W. Jones, and R. H. Hill, *J. Mater. Chem.* **17**, 2206 (2007).
⁴¹V. F. Puentes, P. Gorostiza, D. M. Aruguete, N. G. Bastus, and A. P. Alivisatos, *Nat. Mater.* **3**, 263 (2004).
⁴²J. M. Kinsella and A. Ivanisevic, *Langmuir* **23**, 3886 (2007).